Dissection of the Recognition Properties of p38 MAP Kinase. Determination of the Binding Mode of a New Pyridinyl−Heterocycle Inhibitor Family

Robert Soliva,[†,‡,§] Josep Lluis Gelpí,[†,‡,⊥] Carmen Almansa,[§] Marina Virgili,[§] and Modesto Orozco*[,†,‡,⊥,#]

Departament de Bioquímica i Biologia Molecular, Facultat de Química, Universitat de Barcelona, Martí i Franquès 1, Barcelona 08028, Spain, Molecular Modeling and Bioinformatics Unit, Institut de Recerca Biomédica, Parc Científic de Barcelona, Josep Samitier 1-5, Barcelona 08028, Spain, Drug Discovery, J. Uriach y Cia, Camí Reial 51-57, Poligon Industrial Riera de Caldes, Palau de Plegamans, Barcelona 08184, Spain, Computational Biology Program, Barcelona Supercomputing Center, Jordi Girona 31, Edifici Nexos II, Barcelona 08028, Spain, and Structural Bioinformatics Node, Instituto Nacional de Bioinformática, Parc Científic de Barcelona, Josep Samitier 1-5, Barcelona 08028, Spain

Received September 12, 2006

The main recognition characteristics of the ATP binding site of p38 mitogen activated protein kinase alpha (p38α MAPK) have been explored by a combination of modeling and bioinformatics techniques, making special emphasis in the characteristics of the site that justifies binding specificity with respect to other MAP kinases. Particularly, we have analyzed the binding mode of a new family of p38 MAPK inhibitors based on the pyridinyl−heterocycle core. This family of compounds has a marked pseudosymmetry and can exist in different tautomeric forms, which makes the determination of the binding mode especially challenging. A combination of homology modeling, quantum mechanics, classical docking, and molecular dynamics calculations allowed us to determine the main characteristics defining the binding mode of this new scaffold in the ATP binding site of p38α. A set of free energy calculations allowed us to verify the binding mode proposed, giving an overall excellent agreement with the experimental values. Finally, the binding mode of this new family of compounds was compared to that of other members of the pyridinyl and pyrimidinyl heterocycle class.

Introduction

Tumor necrosis factor-α (TNFα) and interleukin-1β (IL-1β) are two cytokines involved in many basic cellular processes such as response to infectious agents or cellular stress.[1] High levels of these cytokines are also associated with the development of a variety of inflammatory diseases such as Crohn's disease, toxic shock syndrome, rheumatoid arthritis (RA), psoriasis, and inflammatory bowel disease (IBD).[2] Reduction in the levels of TNFα and IL-1β has been recognized as one of the most promising strategies to fight an acute or chronic inflammatory response.[3] The clinical success of Enbrel (Etanercept),[4] a soluble TNF-α receptor, and Remicade (Infliximab),[5] an antibody against TNF-α, in the treatment of RA and IBD has confirmed the utility of this approach. Unfortunately, and despite their success, both Enbrel and Remicade are facing the typical drawbacks associated with a protein therapeutic: high production costs and intravenous administration. This explains the great interest in developing new small molecules able to modulate the levels of TNFα and IL-1β without the problems inherent to the pharmaceutical use of proteins.

A key step in the complex sequence of events leading to the production of TNF-α and IL-1β is the activation of p38 mitogen activated protein kinase (MAPK),[6] a serine/threonine kinase involved in major signal transduction pathways. Activation of p38 MAP kinase is due to upstream MAP kinases like MMK3 and MMK6 which phosphorylate residues Thr180 and Tyr182 located in the activation loop.[6] Once activated, p38 MAPK is able to phosphorylate other downstream kinases, transcription factors, and probably AU binding proteins leading to the production of TNF-α and IL-1β.[7] This whole signal transduction pathway is activated when cells are exposed to a variety of extracellular stimuli ranging from bacterial lipopolysaccharide and UV light to proinflammatory cytokines or growth factors.[8]

P38 MAPK has a large homology with other members of the MAPK superfamily like extracellular signal-regulated kinases (ERK) and c-Jun N-terminal kinases (JNK), with which p38 shares a high sequence identity. These three kinases share a common fold and a high level of sequence identity which handicapped the design of p38 MAPK inhibitors.[8,9] The issue of selectivity is further complicated by the existence of at least four splicing isoforms of p38 (α, β, δ, and γ) which have a large degree of sequence identity, but different tissue distribution, and probably also different functions.[7] Thus, inhibition of the α isoform of p38 MAPK by small molecules becomes an especially challenging task, since a drug must not only bind tightly to the target enzyme but also avoid interaction with other very closely related kinases, which might trigger unpredictable side effects. In this paper, we will try to clarify key differences between the binding site of p38 MAPK and those of other closely related enzymes.

The three-dimensional structure of the complex between p38 MAPK and compound **1** (Figure 1)[10] showed the ATP binding site as the recognition region for the inhibitor. The complex was stabilized by two key interactions: (i) a hydrogen bond between pyridine nitrogen (that mimicking N1 of ATP) and the amide proton of Met109 and (ii) a hydrophobic interaction between the 4-fluorophenyl group and a buried apolar pocket in the protein. Additional contacts were a hydrogen bond between imidazole nitrogen and Lys53 and a π-stacking between the sulfonyl−phenyl group and Tyr35, both of which were partly exposed to solvent. This structural knowledge provided the basis

* Corresponding author. E-mail: modesto@mmb.pcb.ub.es. Phone: 34 93 4037156. Fax: 34 93 4037157.
† Universitat de Barcelona.
‡ Institut de Recerca Biomédica.
§ J. Uriach y Cia.
⊥ Barcelona Supercomputing Center.
Instituto Nacional de Bioinformática.

10.1021/jm061073h CCC: $37.00
Published on Web 12/22/2006

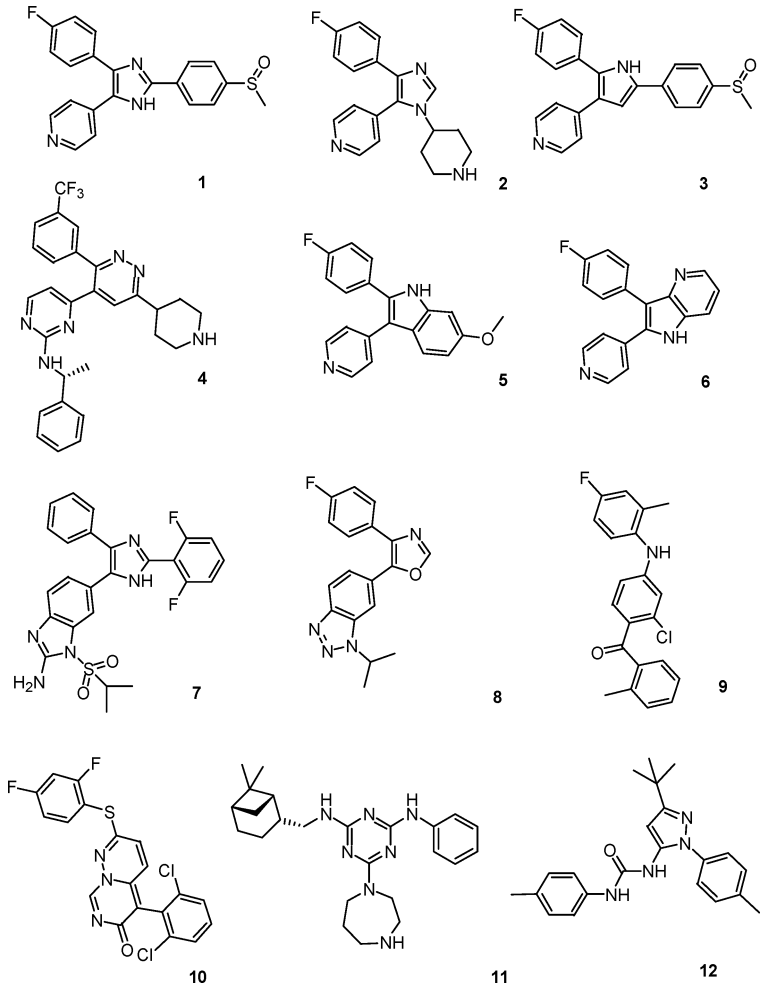

Figure 1. Schematic representation of several known inhibitors of p38α MAPK.

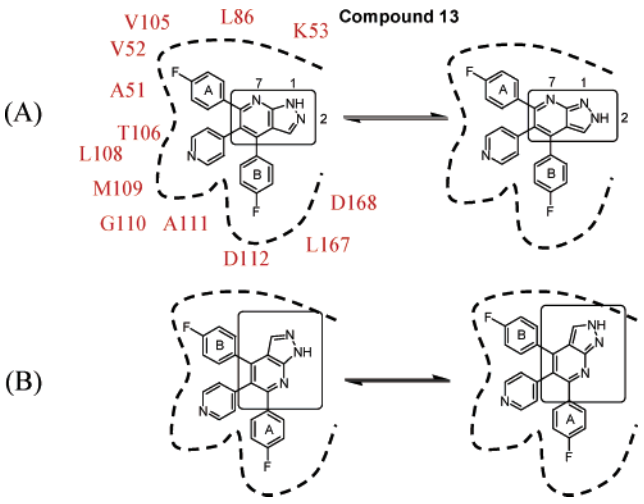

Figure 2. Representation of the four possible binding modes of compound **13** corresponding to the two possible tautomers (N1-H (left) and N2-H (right)) and the two pseudosymmetric arrangements due to 180° rotation around the pyridine−pyrazolopyridine axis (top A, and bottom, B). For the sake of clarity, the central core of the molecule is marked in all cases. Key residues defining the binding pocket are displayed as reference. The numbering scheme for the bicycle nitrogens is also displayed (N1, N2, and N7).

for the design of other imidazole derivatives, such as **2** and also analogues in which the imidazole core was replaced by other five- and six-membered rings such as thiazole, pyrrole **3**, pyrazole, pyridazine **4**, and bicycles such as indole **5** and 4-azaindole **6**, among others (see Figure 1 for examples).[11] They all constitute the pyridinyl−heterocycle class of inhibitors. Close relatives of this family of compounds have been developed in which the pyridine has been replaced by other heterocycles with hydrogen-bond acceptor capability such as 2-amino benzimidazole **7**[12] and benzotriazole **8**.[13] Other families of inhibitors specific for the ATP binding site are based on different scaffolds like the benzophenone **9** and VX-745 **10** (see Figure 1).[14] Although the latter compound and its derivatives display a binding mode similar to compound **1**, its carbonyl group induces a hinge flip and accepts a hydrogen bond, not only from Met109, but also from Gly110. It has been discussed that this feature could be used to gain selectivity against other kinases lacking a Gly at position 110. Other compounds that contact the hinge region via a structural water bridging receptor and inhibitor such as the triaminotriazine **11** have also been developed.[15] Finally, allosteric inhibitors like **12** do not bind to the ATP binding site but into an alternative pocket generated when Phe[169] is flipped out the ATP binding site.[16,17] The recently developed compound **13** (see Figure 2) has been found to inhibit the production of TNF-α and IL-1β through inhibition of p38.[18] Specifically, it showed an IC50 of 161 nM in an enzyme inhibition assay,[19] which suggests that it can be a lead compound for development of a new family of inhibitors. Compound **13** belongs to the pyridinyl−heterocycle group, but it has a unique pseudosymmetrical structure that complicates the determination of the binding mode, since both rings A and B (see Figure 2) could in

principle be fitted in the hydrophobic pocket allowing the formation of the crucial pyridine−methionine hydrogen bond. Furthermore, the pyrazolopyridine could offer two distinct patterns of recognition depending on the tautomeric state of the inhibitor, leading to at least four possible recognition modes for the compound. This multiplicity of possible degenerated binding modes makes the determination of the real anchoring pattern especially complex and challenging.

In this paper we will systematically investigate the recognition properties of the ATP binding site using a large variety of techniques and making special emphasis on the characteristics of the binding site that can be used to increase binding and selectivity in front of other kinases. We will also analyze in detail using state of the art simulation techniques[20−22] the different binding modes for the pseudosymmetric pyridinyl−heterocycle derivatives. We show how once the correct binding mode is determined, quantitative prediction of binding affinities in series of related compounds can be made.

Methods

Molecular Dynamics. The structure of p38α was taken from PDB entry 1A9U, in which the enzyme forms a complex with inhibitor **1**. After removal of this inhibitor, the two tautomeric forms of compound **13** (N1H and N2H) were docked using the appropriate modules of our CMIP program[23] in both A and B (see Figure 2) binding orientations. Docking solutions which do not respect the hydrogen bond with Met109 or do not yield to a proper position of the fluorophenyl group were rejected, and the scored solutions (one for each four different binding modes: A-N1H, A-N2H, B-N1H, and B-N2H) were refined manually trying to increase favorable protein−drug interaction. The second step in the setup of the molecular dynamics (MD) simulation was the placement of counterions, a process crucial to obtain a stable trajectory in proteins showing high density of charges. For this purpose we used the titration module of the CMIP program[23] to add Na^+ and Cl^- until no singularities in the electrostatic potential were found (this implied adding 24 Na^+ and 15 Cl^-). The resulting neutral system was then hydrated by a water cap centered at the OD1 atom of Asn 155, having a radius of 42 Å, ensuring that the whole enzyme was engulfed in solvent. The hydration protocol followed here, quite common in this type of studies, strongly reduces the cost of the simulation without any significant impact on quality, since the process of interest is localized in a small region of the protein. The resulting systems had a total of 8100 residues and around 30 000 atoms.

Parm-98 and TIP3P force fields[24,25] were used to describe interactions for the protein residues, ions, and waters. In order to derive atomic charges for drugs studied here the RESP[26] procedure was used with HF/6-31G(d) wavefunctions obtained considering AM1[27] optimized geometries. Optimal bond lengths and angles were taken from the AM1 optimized structures, while stretching and bending force constants were transferred from the Parm-98 force field. Torsional parameters defining the rotations between the central pyrazolopyridine and the external aromatic rings were parameterized using the PAPQMD procedure[28] from AM1 torsional profiles. The quality of the fitted torsional parameters was verified by comparison with HF/6-31G(d) calculations in selected points of the profiles. All the force field parameters developed here are available upon request to the authors.

The different starting models were first optimized in a sequential process, followed by a thermalization and equilibration protocol.[29] Once they were equilibrated trajectories were followed for 2 ns keeping mobile all water, counterions, the inhibitor, and all residues lining the ATP binding site (group1: residues 27−89, 102−120, 129−190, 193−194, 200−202, 204−209, 211−213, 215−216, 221, 228, and 318−331). This defines a mobile region expanding around 26 Å from the inhibitor binding site. All bond lengths were kept at equilibrium distances using SHAKE,[30] which allowed us to use a 2 fs time step for the integration of Newton's equations. A 12 Å cutoff was used to truncate nonbonded interactions. Simulations were carried out in the isothermic ensemble ($T = 300$ K). The use of restraints to avoid evaporation of solvent particles guarantees that after equilibration, the collected ensemble will not be far from the NVT one.

Some of the MD simulations sampled unstable binding modes (see below), making impossible the determination of average complexes, while others suggested the existence of stable recognition patterns. In the latter case, MD-averaged structures were determined by restricted minimization of the Cartesian average of snapshots collected in the last 0.5 ns of the trajectories.

Free Energy Calculations. Thermodynamic integration (TI) calculations were carried out to determine the difference in binding free energy between two related inhibitors. Following standard thermodynamic cycles, the mutation between inhibitors was performed by using 41 windows both in the complex with the protein and in water. Each window consisted of 5 (or 10) ps of equilibration followed by 5 (or 10) ps of averaging for a total of 410 (820) ps of MD simulation for each mutation both in the bound (protein) or unbound (water) states. The mutations for the bound state of the inhibitors were performed using the equilibrated structures obtained at the end of the 2.0 ns MD simulation. The mutations of the inhibitors in water were performed in cubic systems containing the inhibitor and around a thousand waters, which were previously equilibrated in the NPT ensemble (1 atm, 300 K) using periodic boundary conditions, an integration step of 2 fs, SHAKE, and a 12 Å residue-based cutoff. Technical details of the trajectories used in TI calculations were identical to those used in MD simulations (see above). Final free energy values and their associated standard errors were obtained by averaging the results for the first and second halves of the 410 and 820 ps simulations (i.e., each value reported here is based on four independent free energy estimates). Intramolecular contributions to free energy were explicitly introduced in both protein and solvent calculations and were then corrected using simulations in the gas phase.

Quantum Mechanical Calculations. Compounds based on molecule **13** had different tautomeric possibilities which might yield to different binding modes. In order to determine which is the major tautomer we first computed the relative gas-phase stabilities of compound **13** and also of unsubstituted pyrazolopyridine using ab initio theory,[31,32] at a high level (basis set up to 6-311++G(d) and correlation up to MP4 level; for details see ref 31) which is known to reproduce quantitatively the tautomeric population of these molecules.[33,34] Solvation effects were introduced from gas-phase optimized geometries using our water[35] optimized MST version of the PCM model[36] with all standard parameters. All ab initio calculations were performed using Gaussian 98[37] and Monster-Gauss[38] computer programs.

Active Site Characterization. We first determined key residues for inhibitor binding by computing the interaction energies between the inhibitors and the entire protein. For this purpose we determined[39,40] atom−atom Lennard-Jones and Mehler−Solmayer electrostatic interactions[41] along the last 0.5 ns of the respective MD trajectories. Atomic interactions were then integrated into residues.

Classical molecular interactions (CMIP[23]) were used to characterize the three-dimensional recognition properties of the binding site of p38α MAPK and to compare it with that of other related enzymes. CMIP is a GRID-type calculation, where the (Poisson−Boltzmann) electrostatic and Lennard-Jones interaction energy of the protein with a probe placed in all the positions of a cubic grid centered in the region of interest is computed. To fully characterize the site we considered two charged (O($q = +1e^-$), O($q = -1e^-$) probes, a neutral one O($q = 0$), and a dehydration particle.[42,43] In order to capture the impact of protein flexibility in the definition of binding site recognition properties, CMIP calculations were performed using ensembles of 100 structures collected from the last 1 ns of the trajectory of the protein bound to compound **13** (in

its more favorable tautomeric form and binding mode; see below), which were Boltzmann-weighted as shown in eq 1

$$\mathrm{MIP}_{i,j,k} = E^{\mathrm{vW}}_{i,j,k} + \sum_{s=1}^{N} \zeta^{S}_{i,j,k} E^{\mathrm{ele}}_{i,j,k}(s) \quad (1)$$

where (s) stands for each of the N structures taken from the trajectory and the indexes vW and ele refer to van der Waals and electrostatic interactions, respectively. The Boltzmann-weighted van der Waals and electrostatic contributions are computed as shown in eqs 2 and 3.

$$E^{\mathrm{vW}}_{i,j,k} = -RT \ln N^{-1} \sum_{s=1}^{N} \exp(-E^{\mathrm{vW}}_{i,j,k}(s)/RT) \quad (2)$$

$$\zeta^{S}_{i,j,k} = \frac{\exp(-E^{\mathrm{vW}}_{i,j,k}(s)/RT)}{\sum_{s=1}^{N} \exp(-E^{\mathrm{vW}}_{i,j,k}(s)/RT)} \quad (3)$$

EXTEND-CMIP calculations were also used to determine the regions of possible functionalization of compound **13** to improve binding. For this purpose the CMIP energies between the protein−drug complex (only the active binding mode for the most stable tautomer was considered; see below) and probe particles (neutral carbon and oxygens with +0.1 and −0.1 e charge) were computed as noted above in the presence of inhibitor. To avoid artifactual probe−inhibitor interactions, the charges in the latter were annihilated and the van der Waals radii were scaled by 0.5 to allow the placement of the probe in regions where covalent ligation to the inhibitor is possible.

Comparison with Other Kinases. CMIP calculations were also used to find structural differences between p38α MAPK and other kinases, which could be used to obtain specificity in binding. Comparison was first made with closely related kinases like MAPK p38γ MAPK (60% identity), JNK3 (40% identity), and ERK2 (45% identity). In a second step we introduced in the comparison other kinases which do not belong to the MAPK family and have low homology to p38α MAPK. These included CDK2 (33% identity), GSK3 (26% identity), and cAMP-dependent kinase (25%). CMIP calculations were performed using in all cases the crystal structures of the different enzymes deposited in the PDB[44] and a steric probe (a neutral oxygen). Structures for p38α MAPK, ERK, GSK3, and cAMP-dependent kinase were solved in the absence of ligand, the structures of JNK3 and p38γ MAPK contained an ATP analog at the binding site, and the structure of CDK2 was solved in the presence of an inhibitor (non-ATP analog). In all the cases CMIPs were aligned using the common conserved residues of the ATP binding site.

Results and Discussion

General Binding Site Characterization. The p38α MAPK ATP binding site is located between the large α-rich and the small β-rich domains. The bottom of the binding site cavity is defined by the hinge region connecting the small and large domains. A conserved and very flexible Gly-rich loop, pertaining to the β-rich domain, partially covers the cavity removing water from the region where the adenine of ATP is recognized. Most p38α MAPK inhibitors bind to the adenine subpocket, whose walls are defined by a series of very apolar residues located in the β-rich domain: Val[30], Val[38], Ala[51], Ile[84], Leu[86], Leu[104], Thr[106] (the "gatekeeper" residue at the hinge segment), Leu[108], Met[109]. Residues at the α-rich domain are important for the phosphate and ribose recognition, but in general they do not establish many direct interactions with inhibitors bound to the adenine subpocket (see Figure 3 panel A).

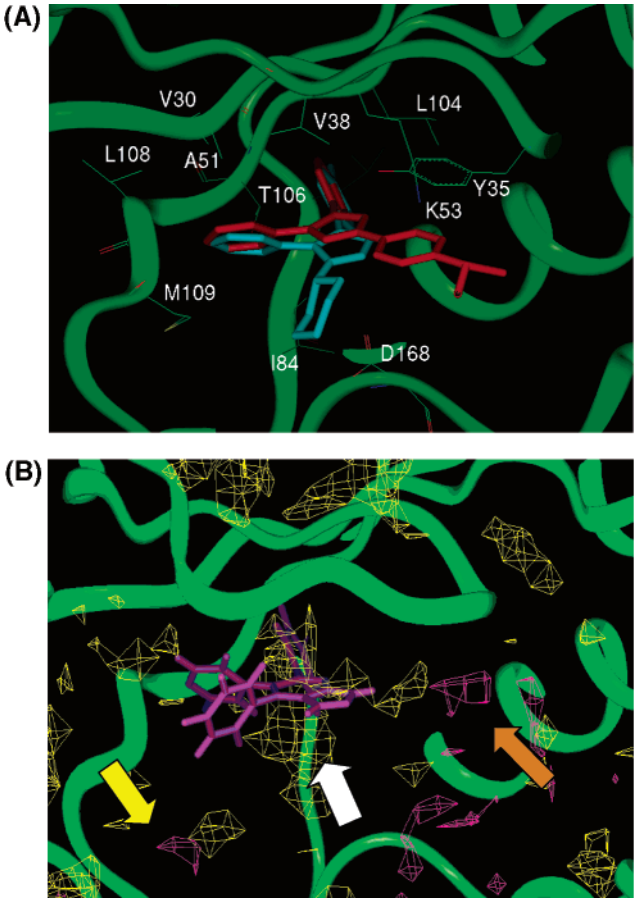

Figure 3. (A) Details of the binding site for compounds **1** (from PDB entry 1A9U in red) and **2** (from PDB entry 1BL7 in cyan). (B) SEDO solvation profiles (yellow 0.1 kcal/mol) and magenta (−3.5 kcal/mol). Arrows indicate the adenine subpocket (white), ribose subpocket (yellow), and phosphate subpocket (orange). As a reference, compound **13** in its suggested binding mode is shown in panel B.

The large number of apolar residues at the adenine subpocket defines a very hydrophobic recognition site, where the removal of water upon inhibitor binding should be easy (see Figure 3 panel B, white arrow). On the contrary, the existence of polar residues at the ribose and especially at the phosphate binding subpockets generates regions of strong solvation in these parts of the ATP binding site (see Figure 3, panel B, yellow and orange arrows), where water removal should have a large energetic penalty. This large asymmetry in polarity defines a quite unique recognition site, which should avoid the anchorage of most undesired ligands.

Since the vast majority of p38α MAPK inhibitors target the ATP binding site, which is largely conserved in different kinases, specificity is a major issue in the development of p38α MAPK inhibitors. CMIP calculations (neutral oxygen as probe) show that, despite the general similarity between the different ATP binding sites, important differences are detected among the kinases analyzed (see Figure 4). Thus, clear differences arise from the fact that p38α MAPK has a wider separation between the Gly-rich loop and the hinge than the other kinases considered in the study. Note that this difference exists not only when the apo form of p38α MAPK is compared with the holo forms of JNK3 and p38γ MAPK, but also for the apo form of other proteins like ERK, GSK3, and cAMP-dependent kinase (see Figure 4) indicating that the differences do not arise from a ligand-induced conformational change at the binding site. In any case, the opening of the gorge between the Gly-rich loop and the hinge and a slightly different orientation of Met[109] in

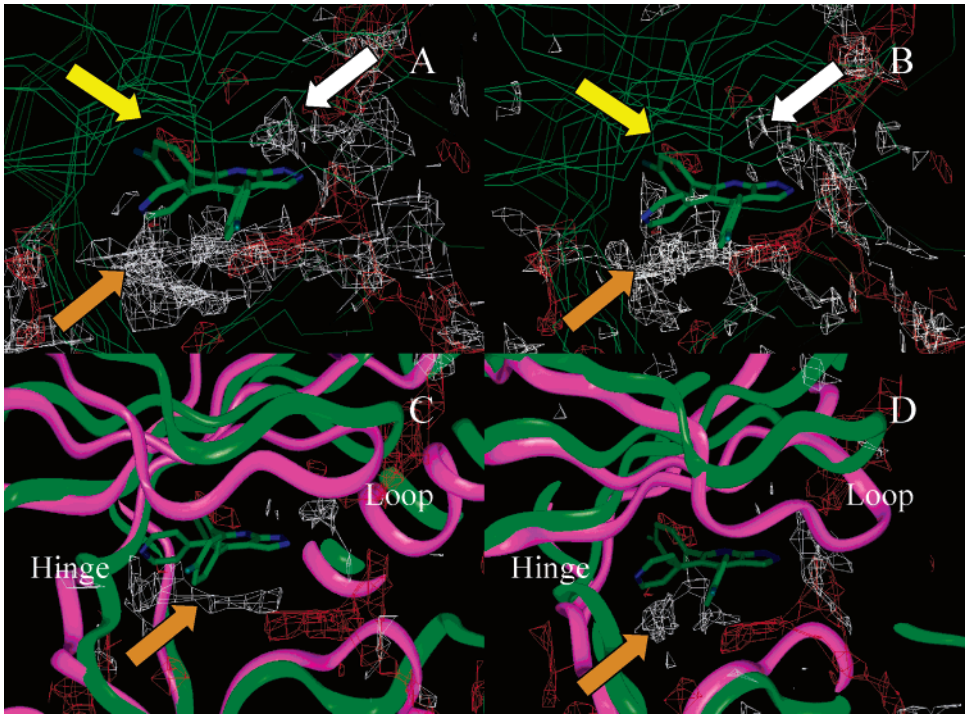

Figure 4. Representation of the −1.5 kcal/mol contour of CMIP (neutral oxygen as probe) for p38α MAPK (red) compared with (A) other MAPKs (white) and (B) related kinases not pertaining to the MAPK family (white). The superposed backbones of the kinases are shown as reference. Detail of the separation between the Gly-rich loop and the hinge in p38α MAPK and two representative kinases are shown in panels C (JNK, a MAPK with 40% identity to p38α MAPK) and D (GSK3, a non-mitogen-activated kinase sharing 33% identity to p38α MAPK). The ribbon of p38α MAPK is shown in green and the other kinases in panels C and D in magenta. In all cases the proposed bound model of compound **13** and the backbones of the superposed proteins are shown as reference. Color arrows are displayed to help discussion in the text.

p38α MAPK and the homologous residues in other kinases generates a differential binding spot for apolar groups in all studied kinases but p38α MAPK, where this position is more solvent-exposed (see white contour marked with an orange arrow in Figure 4). Finally, CMIP contours show the existence of some differences between p38α MAPK and the other kinases around Tyr[35] (see white arrow in Figure 4) which are related to the conformation of the side chain of the residue placed at that position. However, MD simulations (see below) showed that this is a very flexible region and that (at least in the absence of the secondary substrate) the side chain at position 35 can adopt many conformations opening or closing the pocket.

Another differential region between p38α MAPK and the other kinases studied is located around position 106 (the amino acid termed as "gatekeeper"). When Thr is present at that position (p38α MAPK) the protein can accommodate a small aromatic residue in this pocket, but when bulkier groups like Met or Gln are present (like in JNK and ERK), this pocket is collapsed and no aromatic residue can be fitted there (yellow arrows panel A and B Figure 4).[8,11] Clearly this, and the other differences in CMIP between p38α MAPK and related kinases, might be exploited to design specific inhibitors, but caution is needed, since chain rearrangements can open unexpected binding pockets, as recently demonstrated in the crystal structure of JNK3 bound to a derivative of compound **1**.[45]

Determination of Binding/Tautomeric Mode for Compound 13. Virtually all pyridinyl heterocycles reported so far with a bicyclic core are of the type 5 + 6[11] (see for instance compounds **5** and **6**), where the 1-aryl-2-pyridinyl groups branch from the five-membered ring of the bicycle. Compound **13** represents a new 6 + 5 scaffold whose binding mode is unknown. In the lack of X-ray data, modeling is the only approach available for determining the three-dimensional model of interaction of the ligand with the protein. Unfortunately, as noted above, modeling is handicapped by (i) the possible tautomerism of the compound and (ii) its pseudosymmetry, which allows the docking of the molecule with different orientations. Thus, our first step toward the characterization of the binding mode of compound **13** was the analysis of its intrinsic tautomeric properties. For this purpose we performed a high-level ab initio study (see Methods) of the N1H/N2H tautomerism in the pyrazolopyridine group. As a model compound we considered the unsubstituted pyrazolopyridine (see Methods and Figure 2) group, finding a dramatic difference (7.6 kcal/mol) in stability between the major (N1H) and the minor (N2H) tautomer in the gas phase (see Table S1 in the Supporting Information). Comparison of different ab initio estimates (see Table S1) and our previous experience with similar systems[33,34,46,47] strongly suggest that this value is well converged and should be within a few tenths of a kcal/mol from the real one. Solvation reduces the difference in stability between the two tautomers, but the computed difference of stability (2.8 kcal/mol; see Table S1) is large enough to fully guarantee that the N1H is the major tautomer of pyrazolopyridine in water. Calculations repeated using similar techniques (see Methods) with compound **13** provided a picture of the tautomeric equilibrium of the compound close to that of the unsubstituted pyrazolopyridine (see Table S1), the N1H tautomer being the only one detectable in the gas phase (difference of 7.9 kcal/mol to N2H) and the major one in water (difference around 3−4 kcal/mol). The high level of calculation used, the convergence in the results, the similarity with the values obtained using the model system, and our previous experience with related systems allow us to be very confident on the accuracy of these estimates.

Two possible binding modes (A and B; see Figure 2) can be found in docking experiments (see Methods) for the two tautomers of compound **13**. Both binding modes lead to almost

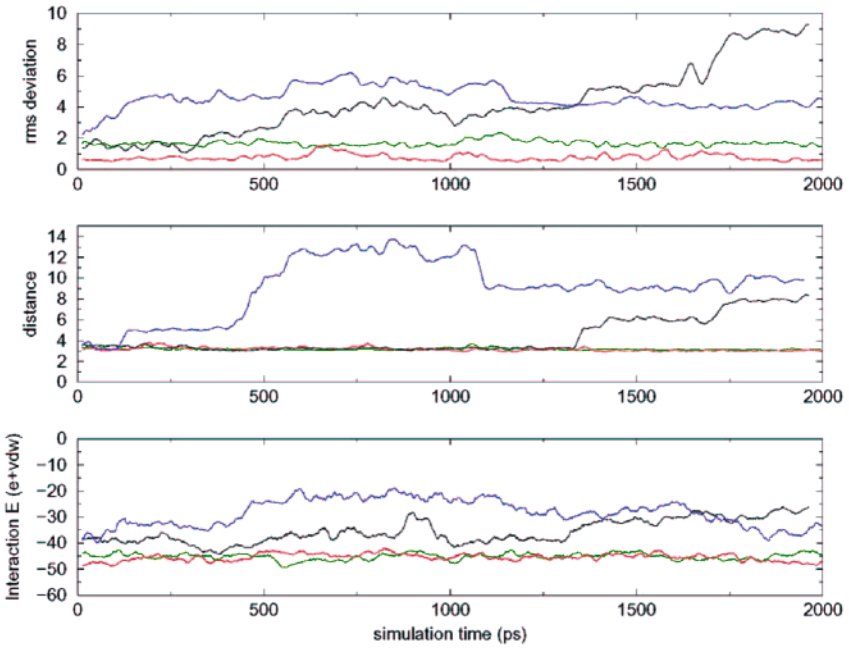

Figure 5. Different indicators of the two binding modes (A and B) for the two tautomeric forms (N1H and N2H). Here, rmsd refers to the root mean square deviation (in angstrom) of the drug with respect to the starting docking position. Distance refers to the separation (in angstrom) between the pyridine nitrogen of compound **13** and the amide nitrogen of Met[109]. Finally, interaction energies refers to electrostatic + van der Waals drug−protein interactions (in kcal/mol) computed as described in Methods. Blue, B-N2H; red, A-N2H; black, B-N1H; green, A-N1H.

identical drug−protein interactions in all the molecules except in the pyrazolopyridine moiety. For binding mode A the pyrazolo ring is pointing to the exterior of the protein, while in binding mode B it is pointing toward Lys[53]. Inspection of previous compounds known to be active does not provide a clue on the real binding mode, since compounds like **6** seem to support binding mode B, while compounds **1** or **5** apparently agree better with binding mode A. Thus, in order to determine the preferred binding mode we performed 2 ns MD simulations for the binding modes A and B. Even after verifying that the N1H tautomer appeared as the most stable one, we could not discard the existence of strong protein interactions stabilizing tautomer N2H. Thus, 4 simulations were performed combining the two binding modes and the two tautomers (i.e., simulations A-N1H, A-N2H, B-N1H, and B-N2H). Monitoring of the rmsd of the drug from binding site, of the drug−protein interaction energy, and of the key hydrogen bond between the pyridine nitrogen and the amino group of Met109 clearly favors (see Figures 2 and 5) binding mode A (for either tautomeric form). Our results strongly suggest that binding mode B should not play a major role in the binding of compound **13** to p38α MAPK. This hypothesis will be further confirmed by additional MD/TI calculations (see below) on compound **13** derivatives.

Assuming that the important binding mode is A, we still need to verify whether or not the protein shifts (from N1H to N2H) the tautomeric preference of compound **13** in its environment. Inspection of trajectories A-N1H and A-N2H does not help us to determine which tautomer is favored by the protein, since both trajectories appear stable. Thus, we performed free energy simulations where the N1H tautomer was mutated to the N2H one and vice versa. After repeating these mutations several times (see Methods) we arrived to a converged value for the "protein solvation effect" of 4.6 ± 0.3 kcal/mol (see Figure 6). This value is not far from that obtained for unspecific water solvation of compound **13** (Table S1), which apparently disagrees with the fact that the N2H tautomer points the two lone pairs (those of N7 and N1) toward Lys[53] as compared to only one lone pair (that of N7) for the N1H tautomer. However, a detailed analysis of the trajectories helps us rationalize the MD/TI results since (i) the expected N1—Lys[53] hydrogen bond (for the N2H tautomer) seems quite weak during the dynamics and (ii) a key water molecule bridging Lys[53] and N1H atom (see Figure 7) is found during 100% of the simulation time for the N1H tautomer. Thus, the special plasticity of the binding site and its partial exposure to solvent explains why the enzyme tolerates either hydrogen-bond donors or acceptors at the N7 position. This counterintuitive finding is supported by inspection of monocyclic compounds **1** and **3**, both very active, and where the position equivalent to N7 can be occupied by either a hydrogen-bond donor or acceptor without major impact in binding affinity.

In any case, the "protein solvation effect" is unable to revert the intrinsic tautomeric preference of this molecule, and accordingly compound **13** is bound in the N1H form (the difference of around 3 kcal/mol (Figure 6) guarantees that the role played by the N2H tautomer is negligible). It is worth noting at this point the importance of calculating intrinsic (in vacuo) properties of ligands and not assuming that they are plastic entities which fully adapt their conformations or topologies to the protein architecture. The bioactive conformation/topology of a ligand is a subtle balance of its intrinsic properties in the gas phase and the stabilizing effect of the protein environment.

Characterization of the Binding Mode for Compound 13. After the 2 ns MD relaxation, compound **13** (in binding mode A and N1H tautomeric form) is placed at the ATP binding site as described above, fitting at one position that is close to that found after the docking experiments (see Figure 7). The molecule makes strong favorable interactions with many residues of the protein, and no unfavorable interactions are found (Figure 8), supporting the suggested binding mode and explaining the good inhibitory profile of this molecule. In addition to direct drug−protein interactions there are also some drug−water interactions involving the pyrazolo nitrogen atoms. One of these water molecules bridging N1H and Lys[53] (see the discussion above and Figure 7) is expected to be crucial for stabilizing the pyrazolo ring, precluding the possibility of substituting the N1 group with apolar compounds.

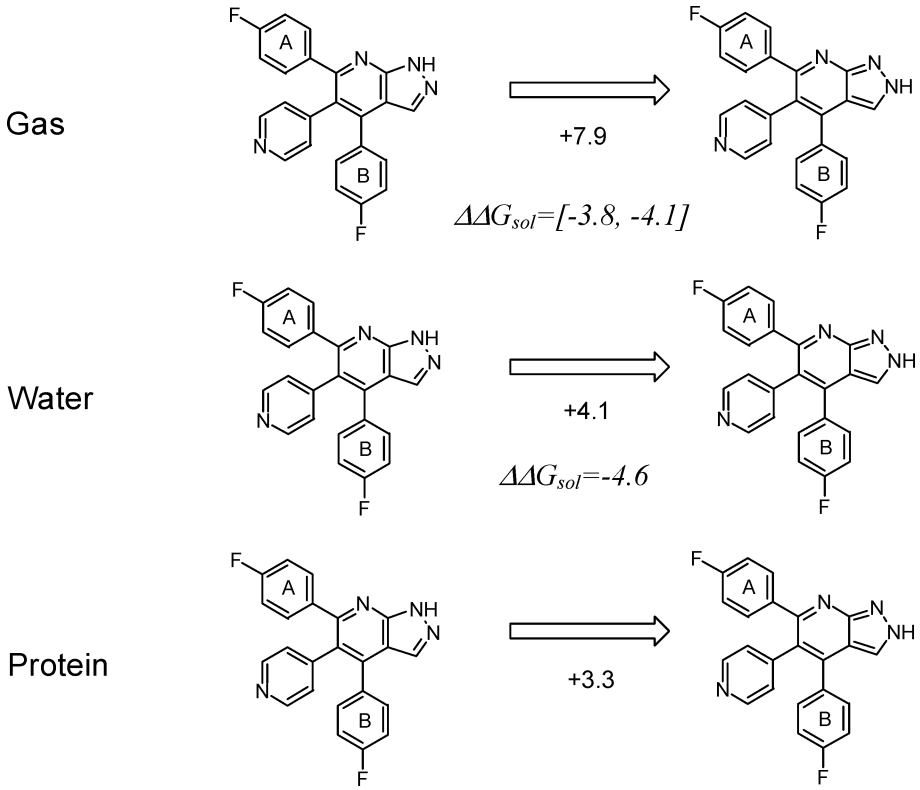

Figure 6. Tautomerization free energies for compound **13** in three different environments. A positive sign means that the N1H tautomer is favored. Numbers in italics correspond to the solvation effect (in water or in the protein). When both MST and MD/TI values are available, the range of values is shown. All values are in kcal/mol.

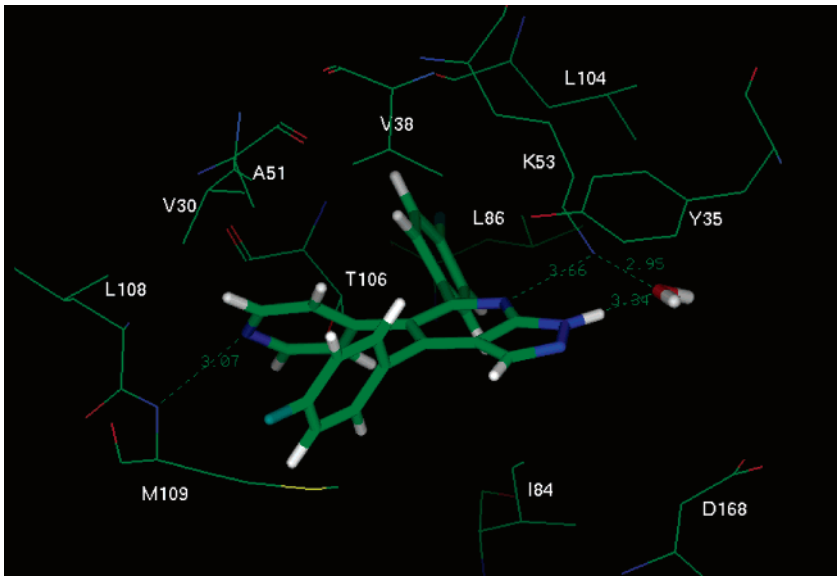

Figure 7. Detail of the optimum binding mode for compound **13** derived from MD simulations (see text). Key interactions, including a water bridge between the drug and Lys[53], are shown.

Interestingly, the drug−protein interaction is dominated by van der Waals interaction, and in fact only two groups display sizable electrostatic interactions with the drug: Lys[53] which (in addition to the water-mediated bridge to N1H) makes a favorable electrostatic interaction with N7 (average distance N(Lys)−N7 around 3.8 Å) and Met[109], which is hydrogen bonded (NH-(Met)−N(Pyr) around 3.0 Å to the drug throughout the trajectory. Around 12 residues of the protein make sizable van der Waals interactions with the drug, mostly with the aromatic rings attached to the pyrazolopyridine core. Very surprisingly, the strongest van der Waals drug−protein interaction is found with Lys[53], whose aliphatic side chain stacks on top of the A-ring (the stability of this type of interaction has been largely discussed in previous works),[48] showing a versatility of Lys residues to establish both polar interactions (via the NH_3^+ group) and apolar interactions (by means of the $(CH_2)_4$ side chain). Other important van der Waals interactions between the drug and the protein are made by apolar residues including Val[30] (interacting with B-ring), Val[38] (interacting with the pyrazolopyridine and A-rings), Ala[51] (interacting with A-ring), Tyr[35] (which stacks with the pyrazolo group), Met[109] (interacting with the pyridine moiety), and Thr[106] (interacting with both A and pyridine rings). As a result of these interactions the three aromatic groups are very tightly bound to the enzyme. Manipu-

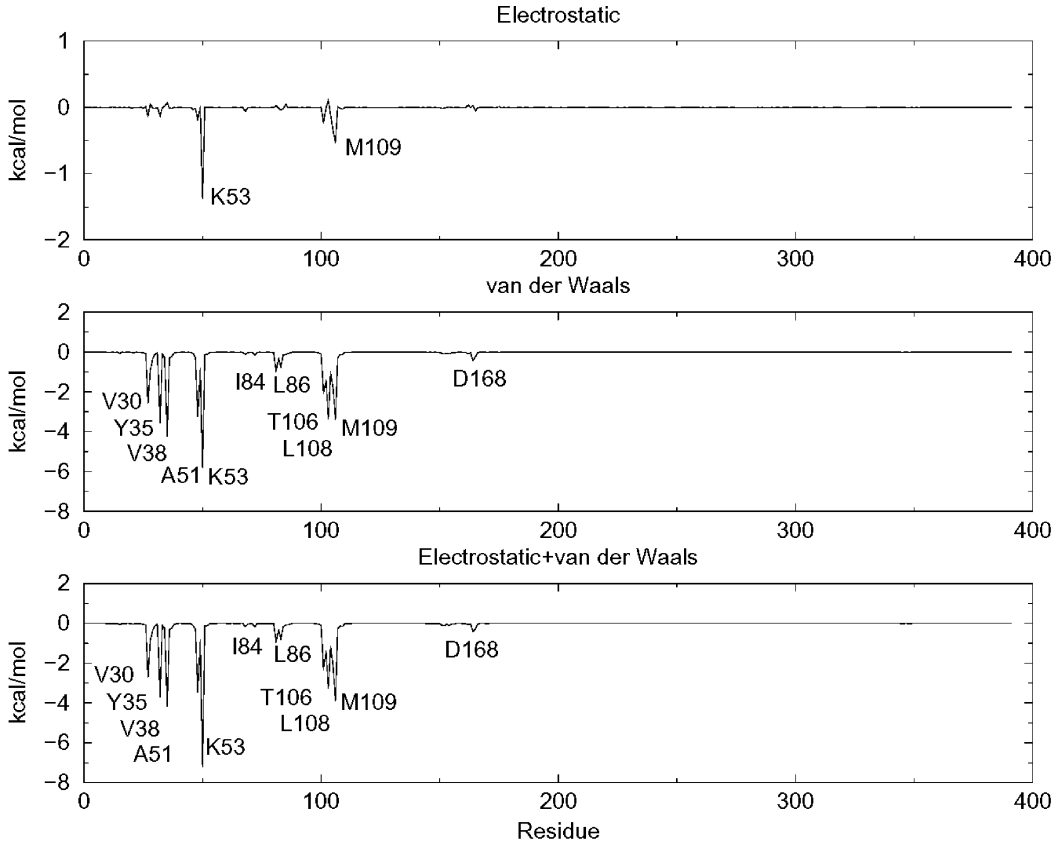

Figure 8. Interaction profiles (see Methods) in kcal/mol for the different residues of p38α MAPK and compound **13**. Key residues for binding are noted in the figure.

lation of these aromatic rings should be done with extreme caution to avoid the generation of molecules which cannot adopt the bioactive conformation.

Compound **13** occupies most of the binding site with the aromatic groups well fitted in mostly hydrophobic pockets, explaining then its good inhibitory properties. Calculations using EXTEND-CMIP methodology (see Methods) considering a neutral probe show that there are no major unfilled pockets near the inhibitor (Figure 9). The only small cavities found appear at the meta/para positions of the A-ring and the meta position of the B-ring (see Figure 9). Interestingly, when the charge of the probe used in the CMIP-EXTEND calculations is shifted from neutral to positive value (see Figure 9, gray and cyan contours) the contour on meta/para-ring A diminishes, while there appears a stronger contour of favorable interaction on meta-ring B. On the contrary, when the charge is shifted from neutral to negative values (see Figure 9, gray and red contours) the contour on meta/para-ring A increases, implying a stronger interaction. Thus, our analysis suggests that slightly electronegative groups should be fit better in meta/para positions of ring A, while slightly electropositive groups appear advisable for the meta position of ring B. Preliminary experimental results obtained in our laboratory (data not shown) demonstrated that introduction of CF_3 at position meta of ring A and CH_3 at the same position of ring B leads to an approximately 3-fold increase in the inhibitory potency over compound **13** giving qualitative support to the binding mode proposed in Figures 7 and 9. There are no direct site-directed mutagenesis experiments on p38α MAPK bound to compound **13** to support our model, but different studies have shown that mutation of Thr^{106} by a bulkier substituent, which removes the binding pocket for ring A, avoids the binding of diarylheterocycles.[49] Additionally, the key role of Lys^{53} in the binding of compound **1** derivatives emerging from our simulations has also been confirmed by site-directed mutagenesis experiments.[50]

As an additional, more quantitative test of the proposed binding mode, we decided to study its ability to describe differential inhibitory properties for derivatives of compound **13** synthesized and analyzed experimentally. For this purpose we computed theoretically (MD/TI) the change in binding free energy upon replacement of compound **13** by related analogs (see Figure 10 and graph S1 of the Supporting Information) assuming binding mode (A-N1H) and compared the estimates with the experimental values[51] Results summarized in Figure 10 show an excellent overall agreement between calculated and experimental measures, giving full support to the binding mode proposed. Thus, methylation at position N2, which will force a lone pair to exist at position N1, favors binding both in MD/TI calculations and experimentally (see Figure 10, compound **15**). Analysis of the binding mode makes clear that this is due to the expected favorable electrostatic interaction between the lone pair at N1 and Lys53 and possibly to the release of the water bridging N1H and Lys^{53}. Substitution of the para F group of ring B by a hydroxyl does not have a major impact on binding (see Figure 10, compound **19**), which is logical considering that this is a mostly solvent-exposed position (see Figure 7). Introduction of a Me− or Cl− group at position C3 of the pyrazolo ring (compounds **14** and **17**) is in general disfavored, which can be expected considering the steric clashes between ring B and the C3-substituent and the fact that, according to the model, this substituent should point to the exterior of the protein and not to a hydrophobic pocket. In summary, the agreement between predicted and experimental $\Delta\Delta G$ of binding between compound **13** and its derivatives strongly support the binding mode proposed, which seems to have predictive power

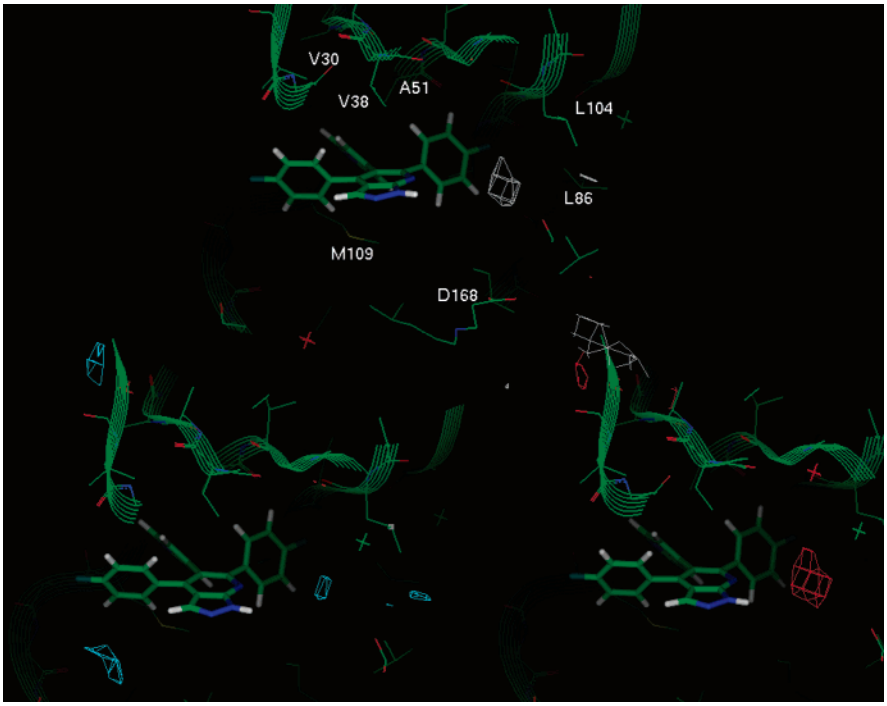

Figure 9. EXTEND maps for compound **13** bound to the binding site of p38α MAPK. Grey, cyan, and red contours correspond to neutral, positive (+0.1), and negative (−0.1) charges, respectively. (Some of the amino acids lining the ATP binding site have been labeled on the top image in order to help discussion in the text.)

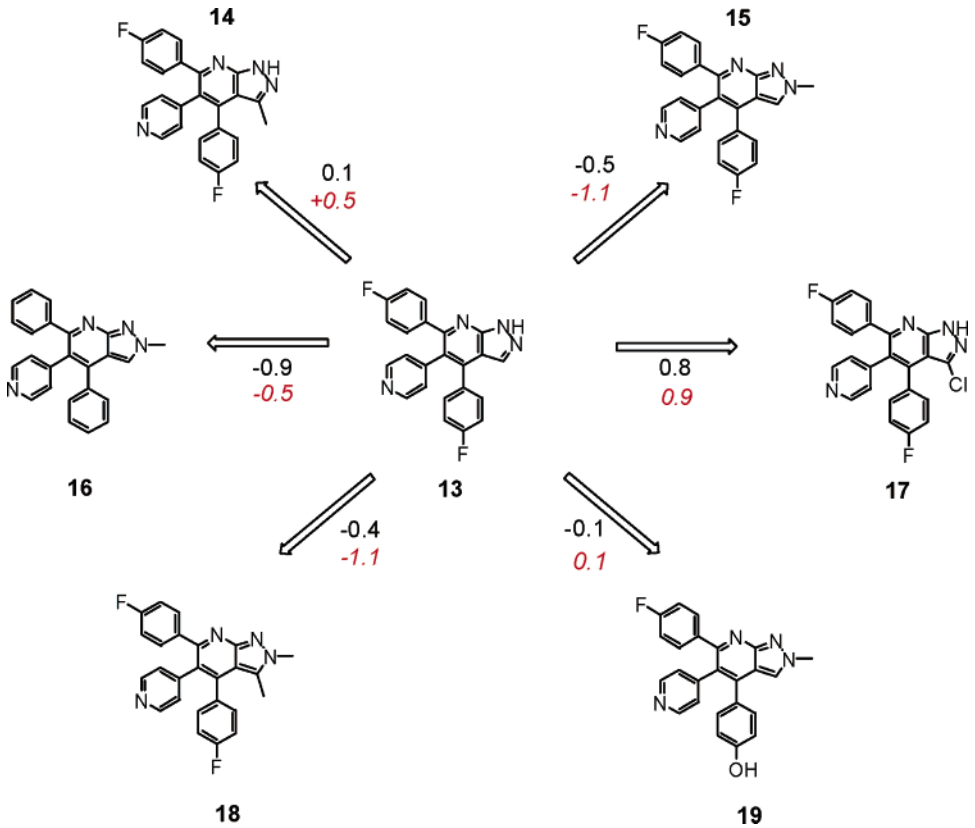

Figure 10. Differential free energies of binding of derivatives of compound **13**. Black numbers refer to MD/TI estimates (typical standard errors are around 0.1−0.2 kcal/mol), while red numbers state the experimental values.

to design new derivatives and underscore the reliability of MD/TI calculations in the prediction of relative free energies of binding.

A final feature worthy of mention for compound **13** is the placement of ring B (Figure 7). This area is pointing away from the protein and into solvent, and when exploited by rigid substituents has traditionally been occupied by more polar moieties such as a piperidine ring (compound 2, Figure 1),[11,52] which interacts via a salt bridge with the conserved Asp168.[52] It is quite interesting that p38 kinase can also accommodate a very rigid and bulky hydrophobic substituent such as a phenyl ring in the same position. This might have an impact on

variables associated to lead optimization such as selectivity and solubility. Because other kinases (see the above discussion) seem to have a narrower, less open and less hydrophobic binding site than p38, this phenyl ring might not always be tolerated in other members of the family. Also, traditionally the solubilizing agents for this class of p38 inhibitors have been placed elsewhere in the molecule (for instance in the sulfonyl−phenyl part in the case of compound **1**). The fact that the 4-hydroxy-substituted phenyl (compound **19**, Figure 10) is nearly equipotent to compound **13** is indicative that this position can be altered in search of new physicochemical properties without decreasing potency.

Ultimately the profile of this novel pyridinyl heterocycle p38 MAP kinase inhibitor family will be defined and assessed as more experimental data become available, but our theoretical calculations have shed some light on how this new family of compounds bind to p38 and have allowed us to compare their molecular recognition with other members of the same class.

Acknowledgment. We thank Dr. Xavier Bartrolí for valuable comments. This work has been supported by the Spanish Ministry of Science and Technology (BIO2006-01602 and GENES-project). We thank the computational support of the Catalan Supercomputer Centers and the Barcelona Supercomputing Center.

Supporting Information Available: Table S1 (results of quantum mechanical calculations on the different tautomeric species) and graph S1 (theoretical vs experimental relative free energies of binding for compound **13** and derivatives). This material is available free of charge via the Internet at http://pubs.acs.org.

References

(1) Dinarello, C. A. Inflammatory cytokines: interleukin-1 and tumor necrosis factor as effector molecules in autoimmune diseases. *Curr. Opin. Immunol.* **1991**, *3*, 941−948.
(2) Feldmann, M. L.; Brennan, F. M.; Maini, R. N. Role of cytokines in rheumatoid arthritis. *Annu. Rev. Immunol.* **1996**, *14*, 397−440.
(3) Newton, R. C.; Decicco, C. P. Therapeutic potential and strategies for inhibiting TNF alpha. *J. Med. Chem.* **1999**, *42*, 2295−2314.
(4) Pugsley, M. K. Etanercept: Immunex. *Curr. Opin. Invest. Drugs* **2001**, *2*, 1726.
(5) Bondeson, J.; Maini, R. N. Tumor necrosis factor as a therapeutic target in rheumatoid arthritis and other chronic inflammatory diseases: The clinical experience with infliximab. Remicade. *Int. J. Clin. Pract.* **2001**, *55*, 211.
(6) Lee, J. C.; Laydon, J. T.; McDonnell, P. C.; Gallagher, T. F.; Kumar, S.; Green, D.; McNulty, D.; Blumenthal, M. J.; Heys, J. R.; Landvatter, S. W.; Strickler, J. E.; McLaughlin, M. M.; Siemens, I. R.; Fisher, S. M.; Livi, G. P.; White, J. R.; Adams, J. L.; Young, P. R. A protein kinase involved in the regulation of inflammatory cytokine biosynthesis. *Nature* **1994**, *372*, 739−746.
(7) Kumar, S.; Boehm, J.; Lee, J. C. p38 MAP kinases: Key signalling molecules as therapeutic targets for inflammatory diseases. *Nat. Rev. Drug Discovery* **2003**, *2*, 717−726.
(8) Salituro, F. G.; Germann, U. A.; Wilson, K. P.; Bemis, G. W.; Fox, T.; Su, M. S.-S. Inhibitors of p38 MAP kinase: Therapeutic intervention in cytokine-mediated diseases. *Curr. Med. Chem.* **1999**, *6*, 807−823.
(9) Tong, L.; Pav, S.; White, D. M.; Rogers, S.; Crane, K. M.; Cywin, C. L.; Brown, M. L.; Pargellis, C. A. A highly specific inhibitor of human p38 MAP kinase binds in the ATP binding pocket. *Nat. Struct. Biol.* **1997**, *4*, 311−316.
(10) Boehm, J. C.; Adams, J. L. New inhibitors of p38 MAP kinase. *Expert Opin. Ther. Patents* **2000**, *10*, 25−37.
(11) Jackson, P. F.; Bullington, J. L. Pyridinylimidazole based p38 MAP kinase inhibitors. *Curr. Topics Med. Chem.* **2002**, *2*, 1011−1020.
(12) de Dios, A.; Shih, C.; Lopez de Urald, e. B.; Sánchez, C.; del Prado, M.; Martin Cabrejas, L. M.; Pleite, S.; Blanco-Urgoiti, J.; Lorite, M. J.; Nevill, C. R., Jr.; Bonjouklian, R.; York, J.; Vieth, M.; Wang, Y.; Magnus, N.; Campbell, R. M.; Anderson, B. D.; McCann, D. J.; Giera, D. D.; Lee, P. A.; Schultz, R. M.; Li, L. C.; Johnson, L. M.; Wolos, J. A. Design of potent and selective 2-aminobenzimidazole-based p38alpha MAP kinase inhibitors with excellent in vivo efficacy. *J Med. Chem.* **2002**, *48*, 2270−2273.
(13) McClure, K. F.; Abramov, Y. A.; Laird, E. R.; Barberia, J. T.; Cai, W.; Carty, T. J.; Cortina, S. R.; Danley, D. E.; Dipesa, A. J.; Donahue, K. M.; Dombroski, M. A.; Elliott, N. C.; Gabel, C. A.; Han, S.; Hynes, T. R.; Lemotte, P. K.; Mansour, M. N.; Marr, E. S.; Letavic, M. A.; Pandit, J.; Ripin, D. B.; Sweeney, F. J.; Tan, D.; Tao, Y. Theoretical and experimental design of atypical kinase inhibitors: application to p38 MAP kinase. *J. Med. Chem.* **2005**, *48*, 5728−37.
(14) Cirillo, P. F.; Pargellis, C.; Regan, J. The non-heterocycle classes of p38 MAP kinase inhibitors. *Curr. Topics Med. Chem.* **2002**, *2*, 1021−1035.
(15) Leftheris, K.; Ahmed, G.; Chan, R.; Dyckman, A. J.; Hussain, Z.; Ho, K.; Hynes, J., Jr.; Letourneau, J.; Li, W.; Lin, S.; Metzger, A.; Moriarty, K. J.; Riviello, C.; Shimshock, Y.; Wen, J.; Wityak, J.; Wrobleski, S. T.; Wu, H.; Wu, J.; Desai, M.; Gillooly, K. M.; Lin, T. H.; Loo, D.; McIntyre, K. W.; Pitt, S.; Shen, D. R.; Shuster, D. J.; Zhang, R.; Diller, D.; Doweyko, A.; Sack, J.; Baldwin, J.; Barrish, J.; Dodd, J.; Henderson, I.; Kanner, S.; Schieven, G. L.; Webb, M. The discovery of orally active triaminotriazine aniline amides as inhibitors of p38 MAP kinase. *J. Med. Chem.* **2004**, *47*, 6283−91.
(16) Regan, J.; Breitfelder, S.; Cirillo, P. F.; Gilmore, T.; Graham, A. G.; Hickey, E.; Klaus, B.; Madwed, J.; Moriak, M.; Moss, N.; Pargellis, C.; Pav, S.; Proto, A.; Swinamer, A.; Tong, L.; Torcellini, C. Pyrazole urea-based inhibitors of p38 MAP kinase: From lead compound to clinical candidate. *J. Med. Chem.* **2002**, *45*, 2994−3008.
(17) Pargellis, C.; Tong, L.; Churchill, L.; Cirillo, P. F.; Gilmore, T.; Graham, A. G.; Grob, P. M.; Hickey, E.; Moss, N.; Pav, S.; Regan, J. Inhibition of p38 MAP kinase by utilizing a novel allosteric bindig site. *Nat. Struct. Biol.* **2002**, *9*, 268−272.
(18) Almansa, C.; Virgili, M. Pyrazolopyridine Derivatives. International Patent Application WO 2004076450.
(19) All IC50s referenced in the paper were determined by Upstate Ltd. (ATP concentration of 100 μM in an enzyme competitive inhibition assay).
(20) Kollman, P. A. Free energy calculations: Applications to chemical and biochemical phenomena. *Chem. Rev.* **1993**, *93*, 2395−2417.
(21) Jorgensen, W. L. The many roles of computation in drug discovery. *Science* **2004**, *303*, 1813−1818.
(22) Pearlman, D. A.; Charifson, P. S. Are free energy calculations useful in practice? A comparison with rapid scoring functions for the p38 MAP kinase proteins system. *J. Med. Chem.* **2001**, *44*, 3417−3423.
(23) Gelpí, J. L.; Kalko, S. G.; Barril, X.; Cirera, J.; de la Cruz, X.; Luque, F. J.; Orozco, M. Classical Molecular Interaction Potentials: Improved Setup Procedure in Molecular Dynamics Simulations of Proteins. *Proteins* **2001**, *45*, 428.
(24) Cornell, W. D.; Cieplak, P.; Bayly, C. I.; Gould, I. R.; Merz, K.; Ferguson, D. M.; Spellmeyer, D. C.; Fox, T.; Caldwell, J. W.; Kollman, P. A. Second generation force field for the simulation of proteins, nucleic acids, and organic molecules. *J. Am. Chem. Soc.* **1995**, *117*, 5179−5197.
(25) Jorgensen, W. L.; Chandrasekhar, J.; Madura, J. D.; Impey, R. W.; Klein, M. L. Comparison of sample potential functions for simulating liquid water. *J. Chem. Phys.* **1983**, *79*, 926−935.
(26) Bayly, C. I.; Cieplak, P.; Cornell, W. D.; Kollman, P. A. A well-behaved electrostatic potential based method using charge restraints for deriving atomic charges. *J. Chem. Phys.* **1993**, *97*, 10269−10280.
(27) Dewar, M. J. S.; Zoebisch, E. G.; Healy, E. F.; Stewart, J. J. P. AM1: A new general purpose quantum mechanical molecular odel. *J. Am. Chem. Soc.* **1985**, *107*, 3902−3909.
(28) Aleman, C.; Canela, E. I.; Franco, R.; Orozco, M. A new strategy for the evaluation of force parameters from quantum mechanical computations. *J.Comput. Chem.* **1991**, *12*, 664−674.
(29) The hydrated systems were subjected to 4000 cycles of energy minimization of water hydrogens; (ii) 4000 cycles of energy minimization of all water molecules; (iii) 2000 cycles of energy minimization of the entire system except the protein; (iv) 2000 cycles of energy minimization of waters, counterions, inhibitor, and all residues lining the ATP binding site (group 1), i.e., residues 27−89, 102−120, 129−190, 193−194, 200−202, 204−209, 211−213, 215−216, 221, 228, and 318−331. The optimized systems were thermalized by increasing the temperature from 150 to 300 K in four steps during 50 ps. They were then equilibrated for 100 ps at constant temperature (T = 300 K). Water, inhibitor, counterions, and all the residues in group 1 were allowed to move during the trajectories.
(30) Ryckaert, J. P.; Ciccotti, G.; Berendsen, H. J. C. Numerical integration of the Cartesian equations of motion of a system with constraints: Molecular dynamics of *n*-alkanes. *J. Comput. Phys.* **1977**, *23*, 327−341.
(31) Geometries were optimised at the HF/6-31.G* level, and energy was computed at the MP2/6-311++G(d) and MP4/6-31G(d) level for the unsubstituted bicycle (see Figure 2). In the case of compound **13**, the ONIOM procedure was applied (ref 32), representing the central bicycle as the higher layer at the MP4/6-31G* level and the rest of the molecule at the HF/6-31G* level (see Figure 2).

(32) Dapprich, S.; Komaromi, I.; Byun, K. S.; Morokuma, K.; Frisch, M. J. A new ONIOM implementation in Gaussian 98. Part I. The calculation of energies, gradients, vibrational frequencies and electric field derivatives. *THEOCHEM* **1999**, *461*, 1−21.
(33) Orozco, M.; Luque, J. L. Theoretical study of the tautomerism and protonation of 7-aminopyrazolopyrimidine in the gas phase and in aqueous solution. *J. Am. Chem. Soc.* **1995**, *117*, 1378−1386.
(34) Orozco, M.; Canela, E. I.; Mallol, J.; Lluis, C.; Franco, R. Ab initio study of the protonation and the tautomerism of the 7-aminopyrazolopyrimidine molecule. *J. Org. Chem.* **1990**, *55*, 753−756.
(35) Curutchet, C.; Orozco, M.; Luque, F. J. Solvation in octanol: Parametrization of the continuum MST model. *J. Comput. Chem.* **2001**, *22*, 1180−1193.
(36) Miertus, S.; Tomasi, J. Aproximate evaluations of the electrostatic free energy and internal energy changes in solution processes. *Chem. Phys.* **1982**, *65*, 239−245.
(37) Frisch, M. J.; Trucks, G. W.; Schlegel, H. B.; Scuseria, G. E.; Robb, M. A.; Cheeseman, J. R.; Zakrzewski, V. G.; Montgomery, J. A., Jr.; Stratmann, R. E.; Burant, J. C.; Dapprich, S.; Millam, J. M.; Daniels, A. D.; Kudin, K. N.; Strain, M. C.; Farkas, O.; Tomasi, J.; Barone, V.; Cossi, M.; Cammi, R.; Mennucci, B.; Pomelli, C.; Adamo, C.; Clifford, S.; Ochterski, J.; Petersson, G. A.; Ayala, P. Y.; Cui, Q.; Morokuma, K.; Malick, D. K.; Rabuck, A. D.; Raghavachari, K.; Foresman, J. B.; Cioslowski, J.; Ortiz, J. V.; Baboul, A. G.; Stefanov, B. B.; Liu, G.; Liashenko, A.; Piskorz, P.; Komaromi, I.; Gomperts, R.; Martin, R. L.; Fox, D. J.; Keith, T.; Al-Laham, M. A.; Peng, C. Y.; Nanayakkara, A.; Gonzalez, C.; Challacombe, M.; Gill, P. M. W.; Johnson, B.; Chen, W.; Wong, M. W.; Andres, J. L.; Gonzalez, C.; Head-Gordon, M.; Replogle, E. S.; Pople, J. A. *Gaussian 98*, rev. A.7.; Gaussian, Inc.: Pittsburgh, PA, 1998.
(38) Peterson, M.; Poirier, R. *MonsterGauss*; Department of Biochemistry, University of Toronto: Toronto, Canada; version modified by Cammi, R. and Tomasi, J., 1987, and by Luque, F. J. and Orozco, M., 2004.
(39) Kalko, S. G.; Luque, F. J.; Orozco, M. *UBEXTRACT Program*; University of Barcelona: Barcelona, Spain, 2002.
(40) Soliva, R.; Almansa, C.; Kalco, S. G.; Luque, F. J.; Orozco, M. Theoretical studies of the inhibition mechanism of cyclooxygenase-2. Is there a unique recognition site? *J. Med. Chem.* **2003**, *46*, 1372−82.
(41) Mehler, E. L.; Solmajer, T. Electrostatic effects in proteins: Comparison of dielectric and charge models. *Protein Eng.* **1991**, *4*, 903−910.
(42) The dehydration particle is a simple cubic particle (1 $Å^3$ in this work) which is assumed to remove water in its environment. The desolvation penalty is then determined by integrating the solvation density as computed by the SEDO version of the Poisson−Boltzmann method (see ref 43).
(43) Arora, N.; Bashford, D. Solvation energy density occlusion approximation for evaluation of desolvation penalties in biomolecular interactions. *Proteins* **2001**, *43*, 12−27.
(44) Protein Data Bank. http://www.rcsb.org/pdb.
(45) Scapin, G.; Patel, S. B.; Lisnock, J.; Becker, J. W.; LoGrasso, P. V. The structure of JNK3 in complex with small molecule inhibitors: Structural basis for potency and selectivity. *Chem. Biol.* **2003**, *10*, 705−712.
(46) Colominas, C.; Luque, F. J.; Orozco, M. Tautomerism and protonation of guanine and cytosine. Implications in the formation of triplex DNA. *J. Am. Chem. Soc.* **1996**, *118*, 6811−6821.
(47) Trygubenko, S. A.; Bogdan, T. V.; Sponer, J.; Rueda, M.; Orozco, M.; Luque, F. J.; Slavíek, P.; Hobza, P. Correlated ab initio study of nucleic acid bases and their tautomers in the gas phase and aqueous solition.1. Cytosine. *Phys. Chem Chem. Phys.* **2002**, *4*, 4192−4203.
(48) (a) Ribas, J.; Cubero, E.; Luque, F. J.; Orozco, M. Theoretical study of alkyl-PI and aryl-PI interactions. Reconciling theory and experiment. *J. Org. Chem.* **2002**, *67*, 7057−7065. (b) Tsuzuki, S.; Honda, K.; Uchimaru, T.; Mikami, M.; Tanabe, K. Origin of the attraction and directionality of the NH/PI interaction: Comparison with the OH/PI and CH/PI interactions. *J. Am. Chem. Soc.* **2000**, *122*, 11450.
(49) Gum, R. J.; McLaughlin, M. M.; Kumar, S.; Wang, Z.; Bower, M. J.; Lee, J. C.; Adams, J. L.; Livi, G. P.; Goldsmith, E. J.; Young, P. R. Acquisition of sensitivity of stress-activated protein kinases to the p38 inhibitor, SB203580, by alteration of one or more amino acids within the ATP binding pocket. *J. Biol. Chem.* **1998**, *273*, 15605−15610.
(50) Young, P. R.; McLaughlin, M. M.; Kumar, S.; Kassis, S.; Doyle, M. L.; McNulty, D.; Gallagher, T. F.; Fisher, S.; McDonnell, P. C.; Carr, S. A.; Huddleston, M. J.; Seibel, G.; Porter, T. G.; Livi, G. P.; Adams, J. L.; Lee, J. C. Pyridinyl imidazole inhibitors of p38 mitogen-activated protein kinase bind in the ATP site. *J. Biol. Chem.* **1997**, *272*, 12116−12121.
(51) The experimental relative free energies of binding were approximated based on the IC50s of compound **13** and its derivatives by $\Delta\Delta G^{A-B}_{Binding} = RT \ln(IC_{50}{}^{A}/IC_{50}{}^{B})$.
(52) Dominguez, C.; Tamayo, N.; Zhang, D. P38 inhibitors: beyond pyridinylimidazoles. *Expert Opin. Ther. Patents* **2005**, *15*, 801−816.

JM061073H